JOURNAL OF THERMOPHYSICS AND HEAT TRANSFER
Vol. 24, No. 2, April–June 2010

Asymptotic Behavior of a Storage Unit Undergoing Cyclic Melting and Solidification Processes

T. Kousksou*
Université de Pau et des Pays de l'Adour, 64013 Pau Cedex, France
A. Jamil†
Université Sidi Mohamed Ben Abdellah, 30000 Fès, Morocco
and
P. Bruel‡
Centre National de la Recherche Scientifique, 75794 Pau, France

DOI: 10.2514/1.46721

In this paper, the asymptotic behavior of a thermal latent-energy storage system undergoing periodic charge/discharge cycles is numerically investigated. The system consists of a cylindrical tank, which is randomly packed with spheres having uniform sizes and encapsulating paraffin as phase change material. The working fluid flowing through the bed is pure air. In the main part of this study, the entrance air temperature is supposed to vary in a sinusoidal way with a one-day period. The related governing equations are solved by a control-volume-based finite difference method. First- and second-law-based efficiency indicators are used to characterize the performances of the system. The effects of the phase change material melting point temperature on the energy efficiency and the irreversibility of the system are investigated. It is shown that in all situations, an asymptotic regime of charge/discharge cycles is reached. For a zero-cycle-average Stefan number, the bed proves to behave like a quasi-perfect reject band filter (i.e., it yields a quasi-constant outlet temperature signal). In such a case, the energy efficiency reaches its maximum value, which also corresponds to a maximum of irreversibility. Thus, this indicates that because of such opposite trends, the design of practical systems should be based on a sound compromise, on a case-by-case basis, and between energy and exergy efficiencies on one side and utilization requirements on the other side. Finally, the predictive capability of such a model is assessed in the situation in which a realistic inlet temperature of the working fluid is considered. The predicted time evolution of the outlet temperature of the working fluid proves to be in good agreement with that reported in the selected reference.

Nomenclature

A_f	=	superficial capsule area per unit bed volume, m^{-1}
c	=	specific heat, $J\,kg^{-1}\,K^{-1}$
d	=	outer capsule diameter, m
f	=	phase change material liquid mass fraction
g	=	gravitational acceleration, $m\,s^{-2}$
$I_{N_S}^{Tm}$	=	asymptotic value of $I_{N_S}^{Tm,\,(i)}$
$I_{N_S}^{Tm,\,(i)}$	=	normalized average value of the entropy generation number for cycle i and phase change material melting temperature Tm
$I_{\eta}^{Tm,\,(i)}$	=	energy-based efficiency indicator for cycle i and phase change material melting temperature Tm
I_{η}^{Tm}	=	asymptotic value of $I_{\eta}^{Tm,\,(i)}$
k	=	thermal conductivity, $W\,m^{-1}\,K^{-1}$
L	=	x length of the tank, m
L_F	=	latent heat of phase change material, $J\,kg^{-1}$
N_s	=	entropy generation number
Nu	=	Nusselt number
Ra	=	Rayleigh number
Re	=	Reynolds number
r	=	radial coordinate, m
$\dot{S}_{\text{gen}}$	=	entropy generation rate, $W\,K^{-1}$
s	=	specific entropy of the fluid, $J\,kg^{-1}\,K^{-1}$
T	=	temperature, K
U_f	=	heat transfer coefficient, $W\,m^{-2}\,K^{-1}$
u	=	mean working-fluid velocity, $m\,s^{-1}$
W_A	=	availability of the system during the charge and discharge periods, J
W_D	=	total exergy destroyed throughout the cycle, J
x	=	axial coordinate, m
β	=	phase change material thermal expansion coefficient, K^{-1}
ε	=	porosity of the bed
η	=	first-law efficiency (heat exchanger)
η_1	=	first-law efficiency (storage unit)
μ	=	dynamic viscosity, $kg\,m^{-1}\,s^{-1}$
ρ	=	density, $kg\,m^{-3}$
τ	=	flow transit time, s
ψ	=	second-law efficiency

Subscripts

C	=	charge
D	=	discharge
eff	=	effective
f	=	fluid
j	=	index of a phase change material sphere
ini	=	initial
inl	=	inlet
out	=	outlet

Received 13 August 2009; revision received 12 November 2009; accepted for publication 16 November 2009.

*Laboratoire de Thermique Énergétique et Procédés, Avenue de l'Université, B.P. 1155; Tarik.Kousksou@univ-pau.fr (Corresponding Author).
†École Supérieure de Technologie de Fès, Route d'Imouzzer, B.P. 2427.
‡Laboratoire de Mathématiques et de Leurs Applications.

Superscripts

l	=	liquid
s	=	solid

I. Introduction

EXERGETIC analysis, derived from application of both the first and second laws of thermodynamics, has become an essential part of thermodynamic assessment of various thermal energy systems. Indeed, the sole use of the conventional energy analysis based on the first-law analysis [1,2] does not allow for a qualitative assessment of the various losses occurring in such systems. In return, the second-law analysis provides a realistic evaluation of the system that helps in discriminating between the different alternative ways of operation.

Thermal energy storage is considered as one of the key elements to accomplish energy recovery and utilization of solar energy, industrial waste heat, and offpeak electricity [3,4]. In such systems, the phase change material (PCM) is encapsulated by using different confinement configurations (cylindrical geometries with or without fins, plates, or spherical capsules). The spherical geometry seems to offer a number of advantages, which ranks it among the most attractive methods of encapsulation. Indeed, the spherical capsules are preferred due to 1) their favorable ratio of volume of stored energy to surface of heat transfer and 2) the easiness of their packing into the storage tank with good bed porosity [5,6].

The proper selection of the storage material depends largely on the temperature properties of the primary source of energy. In any case, though, the ideal PCM candidate for storing energy should 1) possess a high latent heat of transformation; 2) be stable, cheap, and widely available; 3) be environmentally friendly; and 4) be compatible with the other materials of the system equipment [7–9].

As far as thermal energy storage systems are concerned, Bejan [10] pointed out that their primary purpose is not to store energy (as suggested by the name), but rather to store useful work (e.g., thermodynamic availability). Based on this, many researchers carried out extensive analyses of latent thermal energy storage systems using the second law of thermodynamics [11–13]. Most of these analyses were limited, though, to study separately a charge and discharge single period and a small number of studies have been devoted so far to study cyclic melting/freezing of simple systems using PCM [1,14]. Gong and Mujumdar [15] were apparently the first authors to analyze alternating melting/freezing processes involving composite multilayer-PCM slabs. For such a configuration, they found that the energy charge/discharge rate could be increased. Gong and Mujumdar [16] further investigated the effect of different layouts of PCM on the charge/discharge rates of thermal energy in the cyclic melting/freezing in composite slabs of multiple PCM. Their results showed that different combinations of the slabs influenced noticeably the enhancement of the energy charge/discharge rates compared to those obtained with single-PCM slabs. Brousseau and Lacroix [17] carried out a numerical analysis of the cyclic behavior of alternative melting/freezing in a multiplate latent heat energy storage exchanger. Their results indicated that the average output heat load during the recovery period was strongly dependent on the minimum operating temperature, the thermal diffusivity of the liquid phase, the thickness of the PCM layer, and the heat transfer fluid inlet mass flow rate and temperature. Hasan et al. [18] carried out experimental and analytical studies of cyclic charge and discharge of latent energy in a planar slab. Krishnan and Garimella [19] developed a numerical model to study the transient response of the latent energy storage system to short pulses in power dissipation. In their study, the performance of the system was quantified by studying the cumulative heat energy absorbed, the maximum temperature observed in the PCM, and the instantaneous heat absorbed. In a recent study, Kousksou et al. [1] followed the exergy-based approach to study the thermal characteristics during a single-charge period of a packed bed made of PCM-filled spherical capsules. They found that the energy efficiency of the system proved to be very sensitive to the choice of the PCM melting temperature. Based on the same overall methodology, the goal of the present contribution is to put now into evidence the cumulative effects (if any) of the irreversible processes on the long-term (asymptotic) behavior of the system subject to periodic melting/freezing cycles. In the first part, the main features of the proposed modeling strategy will be presented. Next, the most important results will be discussed, with a particular emphasis on the characteristics of the long-term behavior of the latent storage system under study. Finally, to assess the prediction capability of the model when using a realistic inlet temperature of the working fluid, the configuration studied experimentally by Arkar and Medved [20] will be simulated.

II. Model of a PCM Heat Storage System

A schematic of the cylindrical bed storage of length L packed with spherical capsules of diameter d equally filled with PCM is presented in Fig. 1. The numerical model presented in Kousksou et al. [1] for a single charge of such a packed bed is applied to the case of periodic charge/discharge cycles. In this model, the bed is considered as a stack of N_{slices} cylindrical slices of thickness Δx (see Fig. 2) through which air is flowing in a laminar way at a constant mass flow rate. The corresponding superficial flow is considered as unidirectional and so is the corresponding bulk velocity. There is no heat transfer between the bed and its surroundings. All the PCM capsules contained in a given slice are supposed to behave in the same way. Hence, it is sufficient to simulate the behavior of one single-PCM capsule per slice in order to take into account the interaction of the working fluid with the spheres contained in each individual slice. The system will be experiencing a global charge whenever the fluid temperature is such that $T_{\text{out}}(t) \leq T_{\text{inl}}(t-\tau)$ and a global discharge whenever $T_{\text{out}}(t) > T_{\text{inl}}(t-\tau)$, where $\tau = L/u$ is the residence time of the working fluid through the bed. The main assumptions of the model concerning the PCM behavior inside a capsule are now recalled:

1) Melting and solidification processes occur at the same constant temperature.

2) The PCM field is supposed to be spherically symmetric.

3) The PCM density ρ_{pcm} does not depend on the PCM phase.

4) The thermophysical properties of the PCM and of the working fluid are temperature independent.

5) The convection effects present in the liquid region of the PCM contained in the spheres are taken into account via the use of an effective conduction coefficient in the energy equation.

Based on these assumptions and indexing by $j(x)$, the sphere representative of all the spheres with which the working fluid is interacting at abscissa x, the energy balance equations for the fluid and the PCM read as the following:

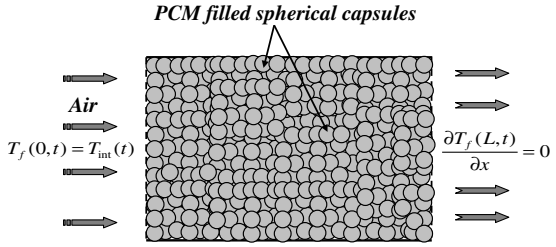

Fig. 1 Schematic of the packed bed.

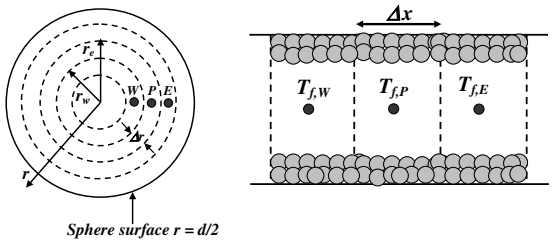

Fig. 2 Radial discretization of a PCM capsule (left, not to scale) and x discretization of the bed (right, not to scale).

Fluid:

$$\varepsilon\rho_f c_f\left(\frac{\partial T_f}{\partial t}+u\frac{\partial T_f}{\partial x}\right)=k_{\text{eff},\,f}\frac{\partial^2 T_f}{\partial x^2}+U_f A_f\left(T_{\text{pcm},\,j(x)}\left(r=\frac{d}{2}\right)-T_f\right);\qquad [0,L] \tag{1}$$

PCM:

$$(\rho c)^*_{\text{pcm},\,j(x)}\frac{\partial T_{\text{pcm},j(x)}}{\partial t}=\frac{1}{r^2}\frac{\partial}{\partial r}\left(r^2 k_{\text{pcm},\,j(x)}\frac{\partial T_{\text{pcm},j(x)}}{\partial r}\right)-\rho_{\text{pcm}}L_F\frac{\partial f_{j(x)}}{\partial t};\qquad r\in\left[0,\ \frac{d}{2}\right] \tag{2}$$

The term $(\rho c)^*_{\text{pcm},j(x)}$ is a function of the PCM liquid mass fraction f given by

$$(\rho c)^*_{\text{pcm},\,j(x)}=\rho_{\text{pcm}}[(1-f_{j(x)})c^s_{\text{pcm}}+f_{j(x)}c^l_{\text{pcm}}] \tag{3}$$

and the thermal conductivity of the PCM is written as

$$k_{\text{pcm},\,j(x)}=(1-f_{j(x)})k^s_{\text{pcm}}+f_{j(x)}k_{\text{eff, pcm}} \tag{4}$$

where the effective thermal conductivity $k_{\text{eff, pcm}}$ of the liquid phase is introduced to take into account the effect of natural convection on the heat transfer during melting. The correlation proposed by Lacroix [21] was retained to express $k_{\text{eff, pcm}}$: namely,

$$k_{\text{eff, pcm}}=aRa^b k^l_{\text{pcm}} \tag{5}$$

where constants a and b are equal to 0.05 and 0.5, respectively. The Rayleigh number Ra is expressed as

$$Ra=\frac{\beta g(\rho c)^l_{\text{pcm}}d^3|T_f-Tm|}{\mu^l_{\text{pcm}}k^l_{\text{pcm}}}$$

where g is the gravitational acceleration, β is the PCM thermal expansion coefficient, μ^l_{pcm} is the dynamic viscosity of the liquid PCM, and Tm is the melting temperature of the PCM. Equations (1) and (2) are coupled via the heat-flux term through the sphere wall [i.e., the last term on the right-hand side of Eq. (1)]. In the expression of that flux, the convection coefficient is calculated by using the relation proposed by Beek [22] and valid for a fluid flowing between spheres arranged in a random form: namely,

$$U_f=\frac{k_f Nu}{d} \tag{6}$$

where the Nusselt number is expressed as

$$Nu=3.22Re^{(1/3)}Pr^{(1/3)}+0.117Re^{0.8}Pr^{0.8} \tag{7}$$

The Reynolds number Re is defined by

$$Re=\frac{\rho_f u d}{\mu_f}$$

and the Prandtl number Pr is given the value 0.71. The effective thermal conductivity of the fluid is defined as $k_{\text{eff},\,f}=0\cdot 5\cdot Re\cdot Pr\cdot k_f$ [23]. The superficial capsule area per unit bed volume A_f is classically expressed as a function of the bed porosity ε and of the capsule diameter d: namely,

$$A_f=\frac{6(1-\varepsilon)}{d} \tag{8}$$

The initial and boundary conditions were chosen as follows

Fluid:

$$T_f(x,0)=T_{\text{ini}},\quad \forall\ x\in[0,L]$$
$$T_f(0,t)=T_{\text{inl}}(t),\quad \frac{\partial T_f(L,t)}{\partial x}=0,\quad \forall\ t>0 \tag{9}$$

PCM:

$$T_{\text{pcm},\,j(x)}(r,0)=T_{\text{ini}},\quad \forall\ r\in\left[0,\frac{d}{2}\right] \tag{10}$$

$$\frac{\partial T_{\text{pcm},\,j(x)}(0,t)}{\partial r}=0,\quad -k_{\text{pcm},\,j(x)}\frac{\partial T_{\text{pcm},\,j(x)}}{\partial r}=U_f(T_{\text{pcm},\,j(x)}-T_f)\quad \text{at } r=\frac{d}{2},\quad \forall\ t>0 \tag{11}$$

The specific characteristics of $T_{\text{inl}}(t)$ related to the cyclic behavior specific to the present study will be given in the next section. In the following sections, whenever possible, the sphere index $j(x)$ will be dropped in order to lighten the notation.

III. Numerical Method

The numerical solution to Eqs. (1) and (2) was based on a cell-centered finite volume approach. As shown in Fig. 2, the x domain $[0,L]$ was uniformly discretized with M_f 1-D control volumes (segments) of length Δx. Each control volume P is delimitated by its eastern E and western W neighbors. Similarly, the r domain $[0,(d/2)]$ of any sphere $j(x)$ was uniformly discretized with M_{pcm} 1-D control volumes (segments) of length Δr (see Fig. 2). Adopting the notations, as well as the same space (upwind scheme for the convection term) and implicit Euler time integration as in Kousksou et al. [1], the resulting final system to be solved was cast under the following tridiagonal generic form (where superscript 0 refers to the previous time-step values):

Fluid:

$$a_{f,\,P}T_{f,\,P}=a_{f,\,W}T_{f,\,W}+a_{f,\,E}T_{f,\,E}+a^0_{f,\,P}T^0_{f,\,P}+b_f \tag{12}$$

with

$$a_{f,\,P}=a^0_{f,\,P}+a_{f,\,W}+a_{f,\,E}+U_f A_f\Delta x \tag{13}$$

where the coefficients were given by [1]

$$a^0_{f,\,P}=\varepsilon\rho_f c_f\frac{\Delta x}{\Delta t},\qquad a_{f,\,W}=\frac{k_{\text{eff},f}}{\Delta x}+\varepsilon\rho_f c_f\frac{u}{2}$$
$$a_{f,\,E}=\frac{k_{\text{eff},f}}{\Delta x}-\varepsilon\rho_f c_f\frac{u}{2},\qquad b_f=U_f A_f T_{\text{pcm}}\left(\frac{d}{2},t\right) \tag{14}$$

PCM:

$$a_{\text{pcm},\,P}T_{\text{pcm},\,P}=a_{\text{pcm},\,W}T_{\text{pcm},\,W}+a_{\text{pcm},\,E}T_{\text{pcm},\,E}+a^0_{\text{pcm},\,P}T^0_{\text{pcm},\,P}+b_{\text{pcm}} \tag{15}$$

with

$$a_{\text{pcm},\,P}=a^0_{\text{pcm},\,P}+a_{\text{pcm},\,W}+a_{\text{pcm},\,E} \tag{16}$$

where the coefficients were given by [1]

$$a^0_{\text{pcm},\,P}=\rho_{\text{pcm}}c_{\text{pcm}}\left(\frac{r_E^2-r_W^2}{3\Delta t}\right),\qquad a_{\text{pcm},\,W}=\frac{r_W^2 k_{\text{pcm},W}}{\Delta r}$$
$$a_{\text{pcm},\,E}=\frac{r_E^2 k_{\text{pcm},E}}{\Delta r}$$
$$b_{\text{pcm}}=\rho_{\text{pcm}}L_F\left(\frac{r_E^3-r_W^3}{3\Delta t}\right)(f_P(t)-f_P(t+\Delta t)) \tag{17}$$

where r_W and r_E designate the local radius of the P control volume faces and where the PCM liquid fraction. Because the coefficients of

the system to be solved are evaluated implicitly, an iterative method of resolution based on a standard Thomas algorithm was used to obtain the time-varying solution to the system. During this iterative process, the liquid mass fraction f was updated at each iteration using the method described by Voller [24]: namely,

$$f_P^{k+1}(t) = f_P^k(t) + \frac{a_{\mathrm{pcm},P}^k}{\rho_{\mathrm{pcm}}^k L_F}(T_{\mathrm{pcm},\,P}^k - Tm) \tag{18}$$

where index k corresponds to the current iteration loop. The liquid fraction is corrected at each node using the following expressions:

$$f_P^{k+1} = \begin{pmatrix} 0 & \text{if } f_P^{k+1} < 0 \\ 1 & \text{if } f_P^{k+1} > 1 \end{pmatrix} \tag{19}$$

Further details concerning the numerical implementation of the present enthalpic phase change method may be found in the work of Voller [24]. At each time step, convergence was assumed to be reached as soon as the temperature residuals fell below some predefined values tol_f and $\mathrm{tol}_{\mathrm{pcm}}$: that is,

$$\left|\frac{T_{f,\,P}^{k+1} - T_{f,\,P}^k}{T_{f,\,P}^k}\right| < \mathrm{tol}_f$$

and

$$\left|\frac{T_{\mathrm{pcm},P}^{k+1} - T_{\mathrm{pcm},P}^k}{T_{\mathrm{pcm},P}^k}\right| < \mathrm{tol}_{\mathrm{pcm}}$$

After performing preliminary tests aimed at determining the sensitivity of the results to the value of tol_f and tol_{pcm}, all simulations were conducted with $\mathrm{tol}_f = \mathrm{tol}_{\mathrm{pcm}} = 10^{-5}$.

IV. Efficiency Indicators Adapted to Cyclic Melting and Solidification Sequences

The single-cycle analysis presented in [1] was adapted to cope with a sequence of cyclic melting/solidification processes. As far as energy storage is concerned, we recall that the primary objective is to ensure that 100% of the latent energy charge/discharge capability of the system is fully used. Because this can be achieved in different ways involving different paraffins (featuring different melting temperatures Tm), the question than can be raised is how to determine the one to be chosen. The first step in paving the way toward answering that question was to characterize the asymptotic behavior of the system undergoing cyclic charge/discharge processes. In that framework, the recourse to criteria defined on the basis of thermodynamics laws (first and second) and aimed at assessing the efficiency of the system was necessary. We briefly recall hereafter the efficiency criteria that can be defined to characterize the performances of the storage system.

A. First-Law Efficiency

From the point of view of the first law of thermodynamics, the efficiency of the system considered as a storage unit would be the ratio of useful energy output to the total energy input during one given period. Thus, for the case of a complete charging/discharging cycle, the corresponding first-law efficiency of the thermal energy storage system is defined as

$$\eta_1 = \frac{Q_d}{Q_c} = \frac{\int_0^{t_d} \dot{m} c_p (T_{\mathrm{inl}}(t-\tau) - T_{\mathrm{inl}}(t))\,\mathrm{d}t}{\int_0^{t_c} \dot{m} c_p (T_{\mathrm{out}}(t) - T_{\mathrm{inl}}(t-\tau))\,\mathrm{d}t} \tag{20}$$

where Q_d is the total energy discharged during the cycle (i.e., extracted from the storage material during the heat recovery process), Q_s is the total energy charged during the cycle (i.e., stored by the phase change material during the heat storage process), and $\dot{m}$ is the mass flow rate of the heat transfer fluid. But for most of the configurations considered here (inlet temperature sinusoidal signals, insulated system, identical latent heat of melting, and solidification of the phase change materials), as soon as the permanent periodic regime is attained, Q_d becomes equal to Q_s and, consequently, the value of η_1 reaches unity. To differentiate between the limit cycle properties featured by the different configurations, the bed will be rather considered as a heat exchanger for which the instantaneous efficiency of the system during the charge/discharge periods will be defined as the ratio between the heat transfer to or from the working flow and the maximum transferable heat: namely,

$$\eta(t) = \frac{|T_{\mathrm{out}}(t) - T_{\mathrm{inl}}(t-\tau)|}{\max|T_{\mathrm{inl}}(t-\tau) - T_{\mathrm{inl}}(t=0)|} \quad \text{for all } t \geq \tau \tag{21}$$

where it is assumed in the denominator that $T_{\mathrm{inl}}(t=0)$ corresponds to the minimum value of $T_{\mathrm{inl}}(t)$ and the maximum is taken over all the cycles. The average efficiency featured by the system over a time interval $[t_1, t_2]$ was simply calculated as

$$I_\eta(t_1, t_2) = \frac{1}{t_2 - t_1}\int_{t_1}^{t_2} \eta(t)\,\mathrm{d}t \tag{22}$$

B. Second-Law Efficiency

The second-law efficiency was based on the calculation of the entropy generation number N_s defined as the degraded exergy (availability) divided by the total exergy input to the cycle: namely,

$$N_S(t_1, t_2) = \frac{W_D(t_1, t_2)}{W_A(t_1, t_2)} \tag{23}$$

where $W_D(t_1, t_2)$ is the total exergy destroyed during the time interval $[t_1, t_2]$ and $W_A(t_1, t_2)$ is the availability of the system during the same time interval. The second-law efficiency ψ was related to N_s by the following relation:

$$\psi(t_1, t_2) = 1 - N_S(t_1, t_2) \tag{24}$$

When $N_S(t_1, t_2)$ is equal to zero, the thermal system achieves its maximum second-law efficiency and approaches a complete reversibility with no availability destroyed. If this is not the case, the availability destroyed is proportional to the instantaneous rate of entropy generation: for example,

$$W_D(t_1, t_2) = T_0\left[\int_{t_1}^{t_2} \dot{S}_g\,\mathrm{d}t\right] \tag{25}$$

where T_0 is the reference temperature chosen such that $T_0 = T_{\mathrm{inl}}(t=0) = T_{\mathrm{ini}}$. The system being considered as open, the instantaneous rate of the entropy generation during the charge/discharge periods was defined as

$$\dot{S}_g = \frac{\partial S}{\partial t} - \dot{m}(s_{\mathrm{inl}} - s_{\mathrm{out}}) \tag{26}$$

where $\partial S/\partial t$ is the instantaneous variation of the entropy of the PCM and the working fluid and s_{inl} and s_{out} are the specific entropy of the fluid at the inlet and outlet of the system such that

$$s_{\mathrm{inl}} - s_{\mathrm{out}} = c_f\,\ell_n\left(\frac{T_{\mathrm{inl}}}{T_{\mathrm{out}}}\right) \tag{27}$$

The entropy variation of the system is the sum of the entropy variation of the PCM and of the working fluid in each control volume: namely,

$$\frac{\partial S}{\partial t} = \sum_{i=1}^{M_f}\left(\frac{\partial S_{f,\,i}}{\partial t} + \sum_{j(i)=1}^{j(i)=M_{\mathrm{PCM}}} \frac{\partial S_{\mathrm{pcm},\,j(i)}}{\partial t}\right) \tag{28}$$

where $j(i)$ is the discrete counterpart of index $j(x)$ introduced in Sec. II. For the working fluid, the entropy variation is given by

$$\frac{\partial S_{f,\,i}}{\partial t} = \rho_f c_f \varepsilon V_i \frac{\partial}{\partial t}(\ell_n\, T_{f,\,i}) \tag{29}$$

For the PCM, whether phase change takes place or not, the entropy variation is

$$\frac{\partial S_{\text{pcm},\,j(i)}}{\partial t} = \delta\left(\frac{\partial f_{j(i)}}{\partial t}\right)(\rho c)^{*}_{\text{pcm}}(1-\varepsilon)V_i\frac{\partial}{\partial t}(\ell_n\, T_{\text{pcm},\,j(i)}) + \left(1-\delta\left(\frac{\partial f_{j(i)}}{\partial t}\right)\right)\frac{(1-\varepsilon)V_{j(i)}\rho_{\text{pcm}}L_F}{Tm}\left|\frac{\partial f_{j(i)}}{\partial t}\right| \tag{30}$$

where

$$\delta\left(\frac{\partial f_{j(i)}}{\partial t}\right)$$

is a Dirac-like function such that

$$\delta\left(\frac{\partial f_{j(i)}}{\partial t}\right)$$

is equal to 1 if

$$\frac{\partial f_{j(i)}}{\partial t} = 0$$

and is equal to 0 otherwise. The availability of the system during the charge/discharge processes observed during the time interval $[t_1, t_2]$ is written as

$$W_A(t_1, t_2) = \int_{t_1}^{t_2} \dot{E}x\, \mathrm{d}t \tag{31}$$

where $\dot{E}x$ is the time rate of exergy change of the system defined by

$$\dot{E}x = (\dot{E}x_{\text{inl}} - \dot{E}x_{\text{out}}) - T_{\text{ini}}\dot{S}_g \tag{32}$$

In this expression, the first and second terms correspond to the transfer rate and destruction rate of exergy, respectively. The rate of exergy transfer is expressed as

$$\dot{E}x_{\text{inl}} - \dot{E}x_{\text{out}} = \dot{m}c_f(T_{\text{inl}} - T_{\text{out}}) - T_{\text{ini}}\dot{m}c_f\,\ell_n\left(\frac{T_{\text{inl}}}{T_{\text{out}}}\right) \tag{33}$$

If N_S is to be used to determine the optimal system configuration, the objective will thus be to minimize the time integral of N_s taken over a representative cycle featured by the system.

V. Results and Discussion

A. Behavior of the Modeled Packed Bed Subject to a Sinusoidal Inlet Temperature

1. *Configuration and Simulations' Parameters*

The system inlet temperature was supposed to vary in a one-day period purely sinusoidal way: namely,

$$T_{\text{inl}}(t) = A\sin(2\pi f t + \theta_0) + K \tag{34}$$

with $f = 1.157 \times 10^{-5}$ Hz. The two constants θ_0 and K were determined by supposing that the inlet temperature at the time origin (i.e., $T_{\text{inl}}(t=0) = T_{\text{ini}}$ was equal to the minimum of T_{inl}). This implies that θ_0 is equal to $-\frac{\pi}{2}$ and that $K = T_{\text{ini}} + A$. Next, the choice $A = T_{\text{ini}}$ led to

$$T_{\text{inl}}(t) = A(\sin(2\pi f t - \frac{\pi}{2}) + 2)$$

Finally, a temperature signal amplitude of 30°C was chosen, which corresponds to $A = T_{\text{ini}} = 15$°C. The different PCM melting temperatures considered, which must obviously belong to the interval [15–45] to be relevant, correspond to the usual paraffins as presented in Zalba et al. [8] and in Abhat [25]. It is possible to define a related average Stefan number

$$\overline{Ste} = |\frac{1}{\hat{T}}\int_0^{\hat{T}} Ste(t)\,\mathrm{d}t|$$

by integrating the Stefan number over a one-day period $\hat{T}$: namely,

$$\overline{Ste} = \left|\frac{1}{\hat{T}}\int_0^{\hat{T}} \frac{\bar{c}_{\text{pcm}}(T_{\text{inl}}(t) - Tm)}{L_F}\,\mathrm{d}t\right| = \left|\frac{\bar{c}_{\text{pcm}}(\bar{T} - Tm)}{L_F}\right| \tag{35}$$

where the average inlet temperature per cycle $\bar{T}$ is equal to 30°C under the present conditions and $\bar{c}_{\text{pcm}}$ is representative of the specific heat capacity of the PCM and was chosen equal to

$$\bar{c}_{\text{pcm}} = \frac{c^l_{\text{pcm}} + c^s_{\text{pcm}}}{2}$$

Table 1 lists the main characteristics of the various paraffins considered. Virtual paraffins were considered in order to reveal some specific behaviors associated to the absence of any phase change in the bed ($Tm = 15$°C or $Tm = 45$°C) or to a zero value of the average Stefan number ($Tm = 30$°C). The x length L of the tank, the capsule diameter d, and the bed porosity ε were equal to 1.5 m, 0.06 m, and 0.4, respectively. If not stated otherwise, the tank was initially assumed to be at a uniform temperature whose level was chosen to be equal to the minimum value of the inlet temperature (i.e., $T_{\text{ini}} = 15$°C) with all the PCM being in a solid state.

2. *Main Features Associated to the Time Evolution of the System*

In all situations, the time evolution of the system was characterized by the presence of an initial transient period followed by a permanent periodic regime. This is illustrated in Figs. 3 and 4, which display the time evolution of the working fluid outlet temperature and of the corresponding mass fraction of liquid PCM in the bed, respectively. Obviously, the duration and the nature of the transient regime are heavily dependent on the value of Tm. Indeed, for the minimum value $Tm = 15$°C, the transient regime corresponds almost entirely to the plateau related to the immediate phase change at constant temperature and the subsequent asymptotic regime is characterized by the absence of phase change in the bed (i.e., the energy storage is uniquely due to the sensible part of the liquid PCM). This is also the case for $Tm = 45$°C, but in that situation, the sensible storage occurs in the solid PCM only (see Fig. 4). From the point of view of energy storage, these two limit cases are obviously far from being optimal for the end user and it should be noted that the melting temperatures for these two cases correspond to the two peaks of $P(T_{\text{inl}})$. The most peculiar behavior, though, is observed for $Tm = 30$°C (i.e., $\overline{Ste} = 0$). In that case, the outlet temperature is almost constant and

Table 1 Main properties and parameters related to the storage system

Paraffins name	Density, kg/m^3	Latent heat of fusion, kJ/kg	Melting temperature, °C	Specific heat capacity, kJ/kg/°C		Average Stefan number over a one-day cycle
				Solid phase	Liquid phase	
Virtual	770.00	236	15.00	2.122	2.219	0.160
Hexadecane	770.00	236	17.10	2.122	2.219	0.138
Heptadecane	775.00	214	21.90	1.947	2.226	0.126
Octadecane	779.00	244	27.10	1.911	2.222	0.069
Virtual	780.50	233	30.00	1.915	2.264	0.000
Nonadecane	782.00	222	32.00	1.920	2.306	0.019
Eicosane	785.00	248	36.60	1.930	2.333	0.057
Virtual	785.00	248	45.00	1.930	2.333	0.130

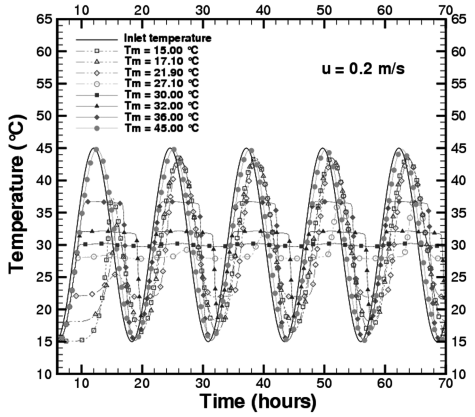

Fig. 3 Time evolution of the working-fluid inlet and outlet temperatures for different PCM melting temperatures (sinusoidal inlet temperature).

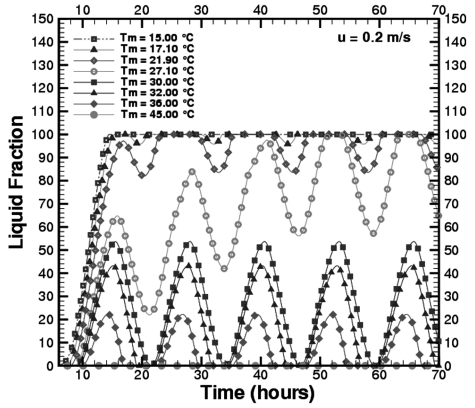

Fig. 4 Time evolution of the PCM liquid mass fraction for different PCM melting temperatures (sinusoidal inlet temperature).

the storage process is essentially latent because the liquid fraction exhibits a saturation-free quasi-sinusoidal temporal behavior. The level of the outlet temperature is close to the cycle average of the inlet temperature (and to Tm because $\overline{Ste} = 0$). Thus, in such a situation, the bed acts as a quite perfect reject band filter centered at the frequency $f = 1.157 \times 10^{-5}$ Hz. Such a quasi-constant outlet temperature feature can be of great interest for many industrial or domestic applications. It should be emphasized, though, that such a behavior was obtained for a very specific symmetric inlet signal, which was moreover invariant from one cycle to another. The present interpretation cannot be readily extrapolated to other type of signals without further investigation. In addition to that, even with the present inlet sinusoidal signal, a velocity change, keeping constant the tank length or vice versa, proved to alter the outlet temperature signal. This is illustrated in Fig. 5, in which it can be seen that a reduction of the transit time achieved through a velocity increase (keeping constant the bed length) leads to the reappearance of some periodic oscillations of the outlet temperature.

For values of Tm below or above 30°C, the asymptotic regime is characterized by a twofold nature of the storage (i.e., latent and sensible). The occurrence of the sensible storage can be identified in Fig. 4 whenever a plateau is observed in the time evolution of the PCM liquid fraction f at a level of either $f = 100\%$ for $Tm < 30$°C or $f = 0\%$ for $Tm > 30$°C. A change of initial conditions proved to only induce a phase shift of the outlet temperature signal with no alteration of the asymptotic signal amplitude time evolution. Indeed, simulations (not shown here) performed for $Tm = 28$°C and for two different initial conditions [i.e., $T_{\text{inl}}(t = 0) = 15$°C and $f = 0$ or $T_{\text{inl}}(t = 0) = 45$°C and $f = 100\%$] show that the two air outlet temperature signals exhibit an identical asymptotic shape with

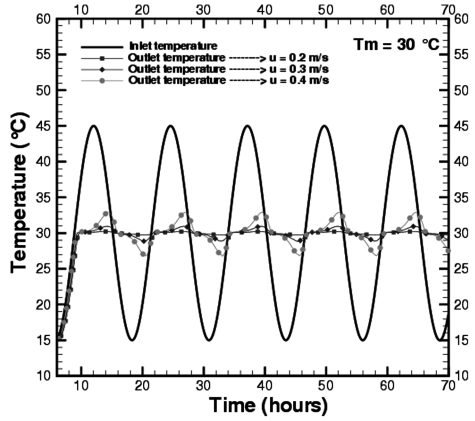

Fig. 5 Sensitivity of the outlet temperature behavior to a mean velocity change (sinusoidal inlet temperature).

simply a phase shift corresponding approximately to a 6 h time lag between them.

The time evolution of the system can always be considered as a sequence of individual global charge/discharge cycles according to the definition given in Sec. II for the relative position of the values of the working-fluid temperatures $T_{\text{inl}}(t-\tau)$ and $T_{\text{out}}(t)$. As this is illustrated in Fig. 6, the 24 h duration of a given cycle (i) will be denoted by $t_c^{(i)} + t_d^{(i)}$ where $t_c^{(i)}$ and $t_d^{(i)}$ correspond to the charge duration (i.e., when $T_{\text{out}}^{(i)}(t) \leq T_{\text{inl}}^{(i)}(t-\tau)$) and the discharge duration (i.e., when $T_{\text{out}}^{(i)}(t) > T_{\text{inl}}^{(i)}(t-\tau)$) of the cycle, respectively. As soon as the asymptotic regime is reached, $t_c^{(i)}$ and $t_d^{(i)}$ do not depend on the cycle index (i) anymore but remain functions of the melting temperature only (for a fixed mean velocity). Last but not least, note that because of the small value of τ (7.5 s for $u = 0.2$ m/s) compared to the period duration, the times $t_0^{(i)}$ seem to correspond to the intersections between the T_{inl} and T_{out} curves, whereas in reality, these instants are slightly shifted from those intersection points by a time interval of τ.

3. *Energetic and Exergetic Efficiencies*

To characterize the various kind of efficiencies (energetic and exergetic) of the system, we shall focus our attention on the asymptotic regimes and more specifically on the limit charge/discharge cycle, which was reproduced periodically in such cases. A criterion was first defined to determine the end of the transient regime or equivalently the beginning of the asymptotic one. With $I_{N_S}^{Tm,(i)}$ being defined as

$$I_{N_S}^{Tm,\,(i)} = \frac{N_s(t_0^{(i)}, t_0^{(i)} + t_c^{(i)}) + N_s(t_0^{(i)} + t_c^{(i)}, t_0^{(i)} + t_c^{(i)} + t_d^{(i)})}{I_{N_S}^{Tm,\,\max}} \quad (36)$$

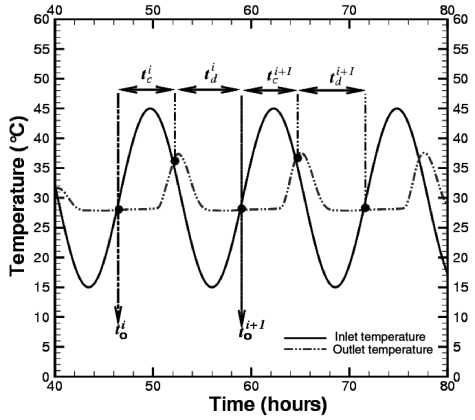

Fig. 6 Asymptotic regime: generic definitions and patterns associated with a charge/discharge cycle (sinusoidal inlet temperature).

a limit regime of charge/discharge cycles was said to be reached as soon as $I_{N_S}^{T_m,\,(i)}$ became independent of the cycle considered. In Eq. (35), $t_0^{(i)}$ denotes the starting time of the ith cycle and $I_{N_S}^{Tm,\max}$ is the maximum of $I_{N_S}^{T_m,\,(i)}$ calculated over all the cycles and for all the melting temperature values. The energy-based efficiency counterpart of $I_{N_S}^{Tm,\,(i)}$ denoted by $I_{\eta}^{Tm,\,(i)}$ was readily defined as

$$I_{\eta}^{Tm,\,(i)} = \frac{1}{t_c^{(i)} + t_d^{(i)}} \int_{t_0^{(i)}}^{t_0^{(i)}+t_c^{(i)}+t_d^{(i)}} \eta(t)\,\mathrm{d}t \tag{37}$$

A specific energy-based efficiency indicator restricted to the charge/discharge period of the cycle can be defined in a similar way: namely,

$$I_{\eta,\,C}^{Tm,\,(i)} = \frac{1}{t_c^{(i)}} \int_{t_0^{(i)}}^{t_0^{(i)}+t_c^{(i)}} \eta(t)\,\mathrm{d}t, \qquad I_{\eta,\,D}^{Tm,\,(i)} = \frac{1}{t_d^{(i)}} \int_{t_0^{(i)}+t_c^{(i)}}^{t_0^{(i)}+t_c^{(i)}+t_d^{(i)}} \eta(t)\,\mathrm{d}t \tag{38}$$

As seen in Fig. 7, where $I_{N_S}^{Tm,\,(i)}$ is plotted against the cycle index (i), only a few cycles were required in all cases to reach the asymptotic regime of charge/discharge cycles. The level of irreversibility (characterized by large values of $I_{N_S}^{Tm,\,(i)}$) was always maximal during the transient regime before relaxing toward its asymptotic lower constant value that will be denoted by $I_{N_S}^{Tm}$ in the following. In all cases, whenever the convergence of $I_{N_S}^{Tm,\,(i)}$ toward $I_{N_S}^{Tm}$ was obtained, so was that of $I_{\eta}^{Tm,\,(i)}$, $I_{\eta,\,C}^{Tm,\,(i)}$, and $I_{\eta,\,D}^{Tm,\,(i)}$ toward their asymptotic values denoted by I_{η}^{Tm}, $I_{\eta,\,C}^{Tm}$, and $I_{\eta,\,D}^{Tm}$, respectively. At several selected times identified in Fig. 8a by labels t_1 to t_8, the spatial evolution of the profile of the liquid PCM mass fraction inside the bed is displayed in Fig. 8b for $Tm = 30°\mathrm{C}$ (where $x^* = x/L$ designates the normalized axial coordinate). Two zones are distinguishable inside the bed. In the first zone, starting from the bed entrance and covering approximately 35% of its length, the melting front exhibits a large amplitude motion with a liquid mass fraction, which may vary locally between 0 and 100% during the cycle. In the second zone, corresponding approximately to the remaining 65% of the bed length, the amplitude of the time evolution of the profile is progressively decreasing when getting closer to the bed exit, where amplitudes of less than 5% are observed. This behavior is consistent with the quasi-constant outlet temperature level of the working fluid observed for that particular case. The presence of such important space and time gradients of the PCM liquid mass fraction inside the bed clearly indicates that the internal layout of the PCM may strongly influence the overall performance of the system. The evolution of the overall exergy-based efficiency of the system $I_{N_S}^{Tm}$ as a function of the melting temperature is presented in Fig. 9. The maximum level of irreversibility is obtained for $Tm = 30°\mathrm{C}$, whereas the predicted minimum values correspond to the absence of any PCM phase change in the bed (i.e., for $Tm = 15°\mathrm{C}$ and $Tm = 45°\mathrm{C}$). In these

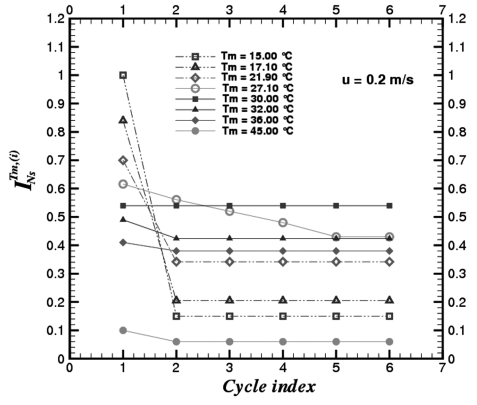

Fig. 7 Cycle-to-cycle evolution of the normalized one-cycle average value of the entropy generation number (sinusoidal inlet temperature).

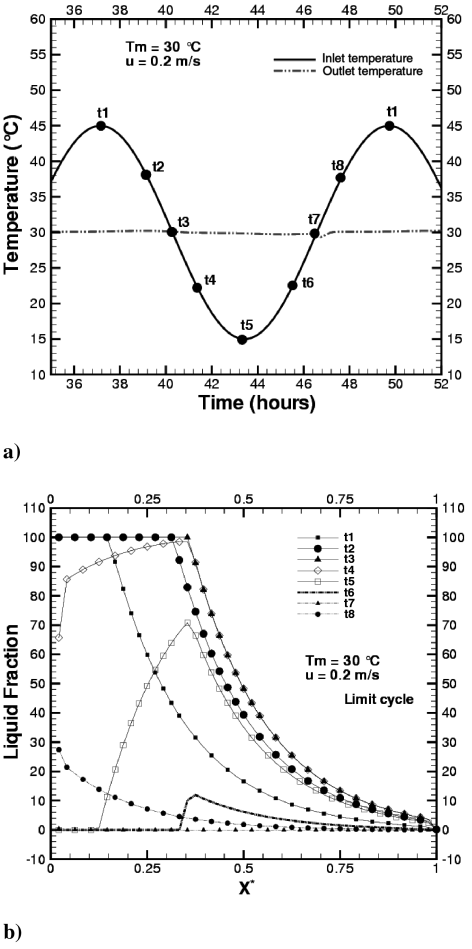

Fig. 8 Asymptotic regime: time evolution of the spatial distribution of the PCM liquid fraction at different selected instants t_i of the limit charge/discharge cycle (sinusoidal inlet temperature).

latter cases, such a low level of irreversibility can be related at first order to the lower level of temperature gradients present in the bed. On the contrary, as it is shown in Fig. 10, this is for the very same melting temperature $Tm = 30°\mathrm{C}$ that the maximum energy-based efficiency was achieved with a value of I_{η}^{Tm} close to 0.24 for such a case. It is also observed that the charge/discharge efficiency factors curves $I_{\eta,\,C}^{Tm}$ and $I_{\eta,\,D}^{Tm}$ are intersecting for $Tm = 30°\mathrm{C}$ at the (common) value of $I_{\eta,\,C}^{Tm} = I_{\eta,\,D}^{Tm} \approx 0.50$. Note also that these curves are not symmetric with respect to the vertical line $Tm = 30°\mathrm{C}$. Such

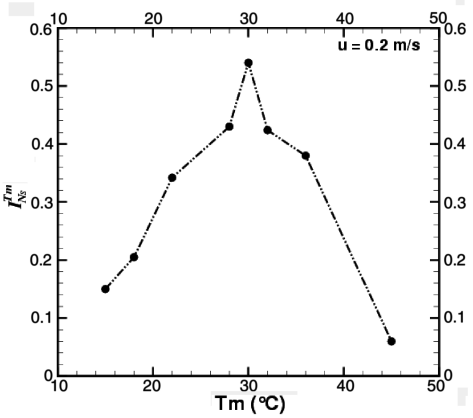

Fig. 9 Asymptotic regime: evolution of the normalized one-cycle average value of the entropy generation number against the PCM melting temperature (sinusoidal inlet temperature).

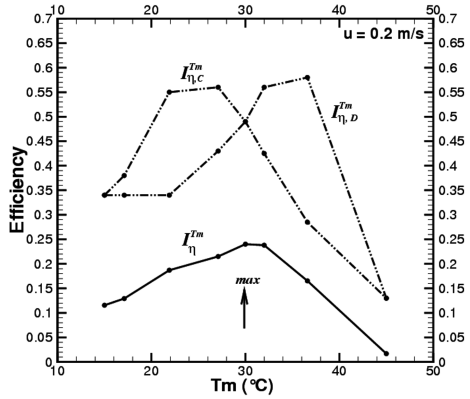

Fig. 10 Asymptotic regime: evolution of the normalized one-cycle average value of the charge, discharge, and global energy-based efficiency indicator (sinusoidal inlet temperature).

asymmetry can be related to the difference in the latent heat of fusion and specific heat capacities of the considered paraffins. It turns out that the most attractive configuration from the point of view of a potential end user (seduced, for instance, by the quasi-constant outlet temperature feature) proved to be unfortunately the one that maximized the degraded exergy level inside the tank. This should be tempered, though, by the fact that it can be expected that when dealing with nonsinusoidal (i.e., real) inlet temperature signals and a complete system, the selection of the proper PCM will result inevitably from a compromise with additional relevant utilization requirements such as 1) the charging/discharging rates and 2) the efficiency of the unit considered as a storage system.

B. Behavior of the Modeled Packed Bed Subject to a Realistic Inlet Temperature

Because the actual solar-radiation-related inlet temperature is periodic but asymmetric between day and night behavior and prone to day-to-day morphology changes, the results obtained previously, necessary to determine the intrinsic behavior of the modeled packed bed, must, nevertheless, be supplemented by a test of the model involving a realistic inlet temperature signal. To achieve this, the configuration experimentally studied by Arkar and Medved [20] was simulated. In their study, the tank length, the capsule diameter, and the bed porosity were equal to 1.52 m, 0.05 m, and 0.388, respectively. The capsules were filled with a RT20 paraffin [26], with melting temperature that was equal to 21.9°C. The simulations were carried out in order to represent the time evolution of the system over a three-day period. As it is visible in Fig. 11, an excellent agreement is observed between the predicted time evolution of the outlet temperature of the working fluid and the measurements.

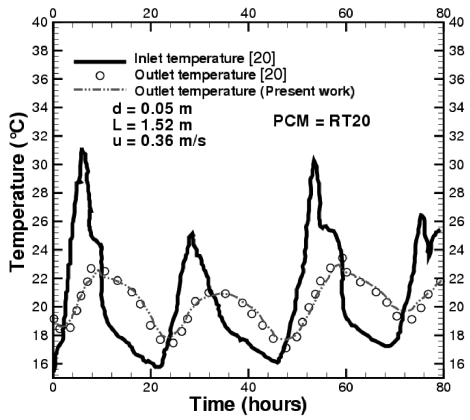

Fig. 11 Time evolution of the working-fluid inlet and outlet temperatures for the RT20 paraffin (real inlet temperature).

VI. Conclusions

The results presented in this contribution show the following:

1) Subject to a sinusoidal inlet temperature evolution of its working fluid, the outlet temperature of a bed packed with paraffin-filled spherical capsules always reaches an asymptotic regime. This asymptotic regime is characterized by a quasi-constant outlet temperature of the working fluid when the average of the Stefan number over one cycle is equal to zero. For such an inlet temperature evolution, the application of efficiency criteria based on an energy analysis (considering the bed as a heat exchanger) and the exergy approach yields opposite trends (i.e., the maximum of energy transfer efficiency is obtained for the minimum exergy efficiency).

2) Subject to a realistic inlet temperature evolution of its working fluid taken from the literature, the predicted time evolution of the working-fluid outlet temperature proved to be in good agreement with that provided by the experiments.

Considering the results obtained in the present study, it seems now relevant to consider the use of the present model to address the question of the integration of such phase change based storage units into a practical system using the solar energy as its primary source. Along these lines, present investigations are now focusing on the optimization of the internal layout of the bed (i.e., the recourse to multiple paraffins), as well as determining how to integrate efficiently such a device into a real system with a particular emphasis on the study of the different aspects linked to the regulation of the thermal loop.

References

[1] Kousksou, T., Strub, F., Castaing Lasvignottes, J., Jamil, A., and Bédécarrats, J.-P., "Second Law Analysis of Latent Thermal Storage for Solar System," *Solar Energy Materials and Solar Cells*, Vol. 91, No. 14, 2007, pp. 1275–1281. doi:10.1016/j.solmat.2007.04.029

[2] Koca, A., Oztop, H. F., Koyun, T., and Varol, Y., "Energy and Exergy Analysis of a Latent Heat Storage System with Phase Change Material for a Solar Collector," *Renewable Energy*, Vol. 33, No. 4, 2008, pp. 567–574. doi:10.1016/j.renene.2007.03.012

[3] Kousksou, T., El Rhafiki, T., Arid, A., Schall, E., and Zeraouli, Y., "Power, Efficiency and Irreversibility of Latent Energy Systems," *Journal of Thermophysics and Heat Transfer*, Vol. 22, No. 2, 2008, pp. 234–239. doi:10.2514/1.31227

[4] Hall, C. A., Glakpe, E. K., Cannon, J. N., and Kerslake, T. W., "Modeling Cyclic Phase Change and Energy Storage in Solar Heat Receivers," *Journal of Thermophysics and Heat Transfer*, Vol. 12, No. 3, June 1998, pp. 406–413. doi:10.2514/2.6352

[5] Kousksou, T., Bédécarrats, J.-P., Strub, F., and Castaing-Lasvignottes, J., "Numerical Simulation of Fluid Flow and Heat Transfer in a Phase Change Thermal Energy Storage," *International Journal of Energy Technology and Policy*, Vol. 6, Nos. 1–2, 2008, pp. 143–158. doi:10.1504/IJETP.2008.017034

[6] Kousksou, T., Bédécarrats, J.-P., Dumas, J.-P., and Mimet, A., "Dynamic Modeling of the Storage of an Encapsulated Tank," *Applied Thermal Engineering*, Vol. 25, No. 10, 2005, pp. 1534–1548. doi:10.1016/j.applthermaleng.2004.09.010

[7] Hadjieva, M., Kanev, St., and Argirov, J., "Thermophysical Properties of Some Paraffins Applicable to Thermal Energy Storage," *Solar Energy Materials and Solar Cells*, Vol. 27, No. 2, 1992, pp. 181–187. doi:10.1016/0927-0248(92)90119-A

[8] Zalba, B., Marín, J. M., Cabeza, L. F., and Mehling, H., "Review on Thermal Energy Storage with Phase Change: Materials, Heat Transfer Analysis and Applications," *Applied Thermal Engineering*, Vol. 23, No. 3, 2003, pp. 251–283. doi:10.1016/S1359-4311(02)00192-8

[9] Huang, M. J., Eames, P. C., and Hewitt, N. J., "The Application of a Validated Numerical Model to Predict the Energy Conservation Potential of Using Phase Change Materials in the Fabric of a Building," *Solar Energy Materials and Solar Cells*, Vol. 90, No. 13, 2006, pp. 1951–1961. doi:10.1016/j.solmat.2006.02.002

[10] Bejan, A., *Advanced Engineering Thermodynamics*, Wiley, New York, 1988.

[11] Dessouky, H. E., and Juwayhel, F. A., "Effectiveness of a Thermal Energy Storage System Using Phase-Change Materials," *Energy Conversion and Management*, Vol. 38, No. 6, 1997, pp. 601–617. doi:10.1016/S0196-8904(96)00072-6

[12] Adebiyi, G. A., and Russell, L. D., "Second Law Analysis of Phase-Change Thermal Energy Storage Systems," *Proceedings of the American Society of Mechanical Engineers*, WA-HTD-80, American Society of Mechanical Engineers, New York, 1987, pp. 9–20.

[13] Saborio, A., Nakamura, H., and Reistad, G. M., "Optimum Efficiencies and Phase Change Temperatures in Latent Heat Storage Systems," *Transactions of the ASME: Journal of Energy Resources Technology*, Vol. 116, No. 1, 1994, pp. 79–96. doi:10.1115/1.2906013

[14] Tabrizi, N. S., and Sadrameli, M., "Modelling and Simulation of Cyclic Thermal Regenerators Utilizing Encapsulated Phase Change Materials (PCMS)," *International Journal of Energy Research*, Vol. 27, No. 4, 2003, pp. 431–440. doi:10.1002/er.886

[15] Gong, Z. X., and Mujumdar, A. S., "Enhancement of Energy Charge–Discharge Rates in Composite Slabs of Different Phase Change Materials," *International Journal of Heat and Mass Transfer*, Vol. 39, No. 4, 1996, pp. 725–733. doi:10.1016/0017-9310(95)00179-4

[16] Gong, Z. X., and Mujumdar, A. S., "Thermodynamic Optimization of the Thermal Process in Energy Storage Using Multiple Phase Change Materials," *Applied Thermal Engineering*, Vol. 17, No. 11, 1997, pp. 1067–1083. doi:10.1016/S1359-4311(97)00012-4

[17] Brousseau, P., and Lacroix, M., "Study of the Thermal Performance of a Multi-Layer PCM Storage Unit," *Energy Conversion and Management*, Vol. 37, No. 5, 1996, pp. 599–609. doi:10.1016/0196-8904(95)00207-3

[18] Hasan, M., Mujumdar, A. S., and Weber, M. E., "Cyclic Meting and Freezing," *Chemical Engineering Science*, Vol. 46, No. 7, 1991, pp. 1573–1587. doi:10.1016/0009-2509(91)87006-X

[19] Krishnan, S., and Garimella, S. V., "Analysis of a Phase Change Energy Storage System for Pulsed Power Dissipation," *IEEE Transactions on Components and Packaging Technologies*, Vol. 27, No. 1, March 2004, pp. 191–199.

[20] Arkar, C., and Medved, S., "Free Cooling of a Building Using PCM Heat Storage Integrated into the Ventilation System," *Solar Energy*, Vol. 81, No. 9, 2007, pp. 1078–1087. doi:10.1016/j.solener.2007.01.010

[21] Lacroix, M., "Numerical Simulation of a Shell-and-Tube Latent Heat Thermal Energy Storage Unit," *Solar Energy*, Vol. 50, No. 4, 1993, pp. 357–367. doi:10.1016/0038-092X(93)90029-N

[22] Beek, J., "Design of Packed Catalytic Reactors," *Advances in Chemical Engineering*, Vol. 3, 1962, pp. 203–277.

[23] Ismail, K. A. R., and Stuginsky, R., Jr., "A Parametric Study on Possible Fixed Bed Models for PCM and Sensible Heat Storage," *Applied Thermal Engineering*, Vol. 19, No. 7, 1999, pp. 757–788. doi:10.1016/S1359-4311(98)00081-7

[24] Voller, V. R., "Fast Implicit Finite-Difference Method for The Analysis of Phase Change Problems," *Numerical Heat Transfer*, Vol. 17, No. 2,1990, pp. 155–169. doi:10.1080/10407799008961737

[25] Abhat, A., "Low Temperature Latent Thermal Energy Storage System: Heat Storage Materials," *Solar Energy*, Vol. 30, No. 4, 1983, pp. 313–332. doi:10.1016/0038-092X(83)90186-X

[26] Arkar, C., "A Parametric Model of a Latent Heat Storage Temperature Response Functions for Natural Heating and Cooling of Buildings," Ph.D. Thesis, Faculty of Mechanical Engineering, Univ. of Ljubljana, Ljubljana, Slovenia, 2006.